Optical Power Measurements in Passive Fiber Optic Networks Using the LoRaWAN Protocol

Danillo F. do Nascimento, Italo R. A. Costa, Rhuan da S. Nunes, José C. do Nascimento

***Abstract*—According to the National Telecommunications Agency (ANATEL), in a report released in 2022, it detailed that around 63% of fixed broadband connections used fiber optic networks for connection. This report demonstrates the constant expansion of fiber optic networks in Brazil. The high demand for optical networks means that internet providers face challenges in delivering a quality service that provides a positive customer experience. As a result, companies in the sector have been looking for solutions to solve problems in connecting optical networks. Currently, in the literature and on the market, there are techniques and tools that enable providers to monitor the network connection, carry out speed tests, promote customer service and carry out preventive maintenance. One of these commercial tools is the Optical Power Meter (OPM), a device capable of taking optical measurements in fiber optic networks. Therefore, this work aims to develop an optical power measurement system for passive fiber optic networks, in order to analyze the quality of the signal provided to users, which uses the LoRaWAN communication protocol, thus integrating with the Internet of Things (IoT).**

***Index Terms*—Fiber Optics; Optical Power Meter; Internet of Things; LoRa.**

I. Introduction

In the age of Information and Communication Technologies, where communication systems have become increasingly crucial to society, the search for efficient and sustainable systems has been the subject of countless studies aimed at improving this tool. This is due to the growing market demand for systems with high connectivity speeds and low failure rates. In this context, an important tool for communication systems is optical networks, which use light signals to transmit information via signals.

According to [1], the first optical tests date back to the mid-1930s, with experiments applied to medicine by the doctor Heinrich Lamm. He carried out tests and experiments to transmit images from light beams conducted by optical fibers. In the 1960s, technological advances made it possible to observe optical signals with the invention of the laser, making it possible to verify the transmission of signals by light beams.

Danillo F. do Nascimento, Italo R. A. Costa, Rhuan da S. Nunes, José C. do Nascimento are linked to the Graduate Program in Electrical and Computer Engineering at the Federal University of Ceará, Sobral, Ceará, Brazil. E-mails: danillo.fernandes03@gmail.com, italorossi.costa@gmail.com, rhuannunes69@gmail.com, claudio@sobral.ufc.br; ORCID: orcid.org/0009-0008-7614-2677, orcid.org/0009-0004-1120-0654, orcid.org/0009-0001-2625-8937, orcid.org/0000-0002-4897-5750.

Submission: 2023-12-21, First decision: 2024-05-03, Acceptance: 2024-08-09, Publication: 2024-08-15.

This article was financed in part by the CAPES - Brasil - Finance Code 001, and BPI FUNCAP.

Digital Object Identifier: 10.14209/jcis.2024.14

Also in this decade, physicists Charles K. Kao and George Hockham published an article describing the possibility of optical fibers transmitting high-capacity signals in communication systems [2]. With Kao and Hockham's efforts, the first optical fiber was manufactured. From this discovery, numerous technologies related to optical fibers emerged.

This discovery gave rise to numerous technologies related to optical fibers. After their manufacture, research focused on improving the performance of optical networks [3]. It was then possible to see the high capacity of these networks for transmitting signals, as well as the improvement in signal quality.

The choice of systems made up of optical networks can be attributed to their conditions and configurations, since they are networks immune to electromagnetic interference, which ensures reliable and stable signal transmission. This is important in industrial or urban environments, where electromagnetic interference can be a significant problem. In [4], it is detailed that the United Nations (UN) has committed to extending the universal broadband network by 2030. There will, therefore, be a significant increase in demand for broadband systems, and with this, optical networks will become increasingly essential to meet society's connectivity needs.

With the growing demand for efficient systems with low failure rates, Internet service providers have invested in research and projects aimed at minimizing problems in optical systems [5]–[9]. Against this backdrop, it is worth noting that the search for quality connections is an essential factor when users choose their internet provider. This has led to the expansion of fiber optic networks, resulting in a significant improvement in the quality of the signal and connection provided by internet providers [7], [9]. Despite this expansion, some challenges have arisen for providers, including difficulties in effectively monitoring signal quality and preventing customer connection losses. This problem can also be attributed to the structure of fiber optic networks, most of which are Passive Optical Networks (PON), which use passive optical splitters as a cost-effective solution and are susceptible to losses in signal quality and optical network failures [6].

Faced with the need to ensure quality signals and efficient connections for users, companies and universities have conducted studies aimed at developing techniques, methods, and solutions to reduce failures in optical systems applied to fiber optic networks [6]. In the commercial sector of optical networks, equipment is available to perform signal quality tests on fiber optic networks, obtaining data and information from the light beams emitted through the optical fibers to check the quality of the signal in areas where users have lost connection. Among these devices is the Optical Power Meter (OPM),

which measures the power of an optical signal transmitted through a fiber cable. The measurements made by the OPM allow for checking whether the optical signal is within the desired parameters or if there has been any significant loss due to local faults [10], [11]. However, the OPM cannot be used to remotely determine where a user's optical signal may have been lost, necessitating the dispatch of a technician to identify the exact point where the signal strength drop occurred.

Among these challenges, a significant gap exists in fiber optic network systems concerning the search for efficient and autonomous solutions for monitoring connection loss in optical networks. This article aims to detail the creation of an optical power measurement system using the LoRaWAN protocol. Among the main long-distance IoT networks [12]–[14], we opted for the LoRaWAN network due to its advantages in terms of low energy consumption, low operating costs, low latency and high flexibility [15], [16].

The system comprises hardware designed to analyze the signal quality of optical networks and identify the exact location of faults using the LoRaWAN communication protocol. This system will enable internet providers to conduct maintenance promptly, aiming to restore the signal and enhance the customer experience.

II. Theoretical Foundations

A. Optical Fiber

As detailed in the introduction, Charles K. Kao and George Hockham carried out and published studies that later enabled the creation of fiber optic networks [2]. After Kao and Hockham's conclusions, optical networks advanced significantly. Their application was mainly for telephone networks; in 1973, for example, the first telephone network operating using fiber optic technology was created. With the design of the Ethernet protocol, optical networks were also used for applications in fixed broadband networks [17].

Optical networks applied to the Internet require infrastructure capable of delivering a quality connection to users. They use infrastructures such as the Passive Optical Network (PON), an optical fiber architecture that makes it possible to distribute optical signals for broadband services [18], with the help of Splitters. There is also the Ethernet Passive Optical Network (EPON) and the Gigabyte Passive Optical Network (GPON), which are derived from the PON and differ in the bandwidth rate they transmit.

The PON architecture is widely used in optical networks and was developed with the aim of providing point-to-multipoint access between users and telecommunications networks via fiber optic communication [19]. Fig. 1 details the topology of the PON architecture.

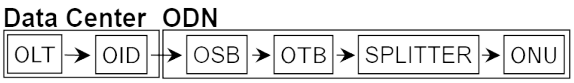

Fig. 1. PON Topology.

The fiber flow begins at the Optical Line Terminal (OLT), which is responsible for providing the PON interface. The fiber is then directed to the Optical Internal Distributor (OID), which is responsible for managing the optical cables. After passing through the OID, the fiber is directed to the Optical Splice Box (OSB), which is a device that seals the splice point, preventing water or other disturbances from entering. After the OSB, the fiber goes to the Optical Terminal Box (OTB), which has the function of protecting the optical splices between the incoming cable and the outgoing cables. Finally comes the Optical Network Unit (ONU), which is where the optical fiber reaches the end user.

B. Splitter

For optical systems to operate and transmit signals effectively, it is necessary to use certain devices to interconnect the systems and amplify the transmission. One of these devices are Splitters, which are responsible for dividing and distributing the optical signal from one optical fiber network to another [20]. The splitter operates in such a way that the Optical Line Terminal (OLT) serves several Optical Network Terminals, generating signal distribution. Splitters are used in PON networks due to their architecture and characteristics, which allow for greater network capillarity [21], [22].

Splitters come in different types and configurations, including balanced and unbalanced splitters. Balanced splitters are used when a balanced network is required. The system operates as follows: when it receives a signal at the input, this signal is split equally to all the outputs [23]. Fig. 2 shows a balanced splitter, where the outputs have equal values

Unbalanced Splitters, as their name suggests, are unbalanced, resulting in a non-uniform distribution of the input signal and, as a consequence, an unbalanced network [23]. Its application is effective in directing more power to a specific region of the network, such as in cases where one branch requires more power than the others. Fig. 3 illustrates the splitting process in an unbalanced splitter, where the outputs have different values.

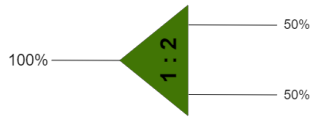

Fig. 2. Balanced Splitter.

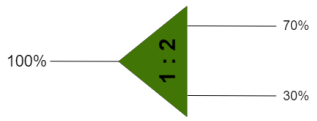

Fig. 3. Unbalanced Splitter.

Splitters are generally assembled and configured in a cascade format, allowing several splitters to be connected in series and optical systems to be expanded to meet different connection demands [24]. Fig. 4 exemplifies one type of cascading, namely 2-level cascading with 16 ports.

The use of devices such as splitters can lead to limitations or problems in optical systems, especially limitations related to power losses during the cascading process [3].

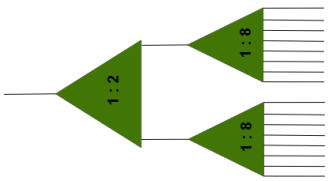

Fig. 4. Cascading Splitters.

C. Photodiode

A photodiode is a semiconductor device that makes it possible to convert light into electric current. The device operates on the photoelectric principle, in which light falling on the semiconductor material generates pairs of electrons [25]. Among the existing photodiodes is the InGaAs photodiode, a semiconductor made up of the elements Indium (In), Gallium (Ga) and Arsenic (As), forming the term InGaAs [26]. The combination of these elements in the semiconductor allows the photodiode to measure wavelengths in the near-infrared region, contributing to applications in optical networks that operate in this spectrum [25].

D. Transimpedance Amplifier

A transimpedance amplifier (TIA) is an electronic device applied to systems where it is desired to convert input current into output voltage [27]. The TIA circuit consists of an amplifier, a feedback resistor (FR) between the output and the inverting input, a capacitor connected in parallel with the feedback resistor and a photodiode, connected in parallel with the inverting and non-inverting inputs, as shown in Fig. 5.

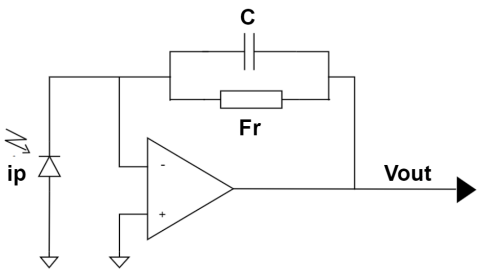

Fig. 5. Transimpedance Amplifier Circuit.

Equation (1) establishes how to calculate the modulus of the output voltage of a circuit with the TIA [28].

$$Vout = FR \times ip \tag{1}$$

Where: *Vout* is the output voltage; *FR* is the feedback resistance; and *ip* is the photogenerated current.

One of the advantages of using a transimpedance amplifier is its high sensitivity to currents, which allows weak signals to be amplified and enables the detection of low signals [27]. However, its application can result in instabilities caused by noise and interference. These issues can be mitigated by incorporating capacitors and resistors to act as filters. In the circuit shown in Fig. 5, capacitor *C* is responsible for stabilizing the output voltage signal [28].

E. Internet of things

Internet of Things (IoT) systems aim to create a network where all objects can connect to the internet and thus collect and share data with each other. The information collected can be used and applied for analysis, automation and improving efficiency in various areas, such as health, transportation, agriculture, manufacturing, among others [29].

Amid the evolution of IoT systems, LoRa, an electronic device capable of wireless communications, has emerged. Its name comes from "LOng RAnge". The device offers long-distance connectivity, coupled with its low power consumption, which makes it an excellent device for IoT applications [29]. The insertion of systems with LoRa contributes directly to data processing and transmission.

III. Proposed Optical System

This topic details the methodologies adopted to develop the optical measurement system. By combining components and software, it was possible to develop the device proposed in this article. Fig. 6 shows a block diagram with the main components used to build and operate the device.

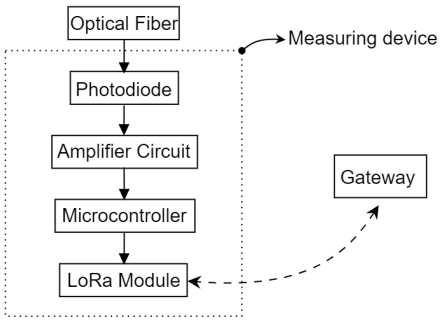

Fig. 6. Overview of the Proposed System.

A. Topology Configurations

For this research, an Optical Line Terminal (OLT) was used to transmit the signal through the optical fiber. Tests were conducted based on the Passive Optical Network (PON) topology, simulating the losses that can occur during the transmission of information through optical fiber.

For this project, we used an OLT from the manufacturer EPON OLT, model V-SOL V1600D16. This component was chosen because of its ability to emit optical signals with a wavelength in the 1490 nm range. The signal emitted by the OLT is routed to the OTB and then distributed via 1/99 unbalanced splitters. The purpose of the split is to preserve the quality of the customers' fiber optic signal by directing only 1% of the power to the measurement device.

To simulate the losses that can occur during signal transmission to the final destination of the optical fiber, the cascading splitters technique was used, allowing for the gradual attenuation of the signal.

During the simulation, an output power of 6 dBm was utilized for the OLT, and a loss of -21.6 dB was applied to simulate the 1% output of the unbalanced 1/99 splitter [30].

According to Fig. 7, the splitters utilized to attenuate the power of the signal from the OLT will be cascaded within the "Attenuation" block. Combinations of balanced splitters were employed, ranging from 1/2 to 1/16, enabling an approximate attenuation of 3.4 dB for each cascading stage. Following attenuation, the signal is directed to the amplification circuit.

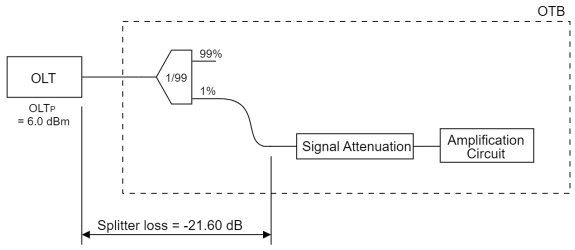

Fig. 7. Signal attenuation with 1/99 splitter.

B. Photodiode and TIA

After the signal is attenuated and sent to the splitter, the signals go to the photodiode and then to the amplification circuit.

To do this, the signal is received by the InGaAs (Indium-Gallium-Arsenic) photodiode, where an electric current proportional to the intensity of the incident light is generated. The Op-Amp converts the photodiode current into an output voltage (Vout). The current generated by the photodiode and Vout have a relationship determined by the feedback resistors (FR). This relationship can be seen from Equation 1.

The voltage generated by the photodiode will be amplified by the Op-Amp. The FR are connected to the switches and are controlled by the microcontroller. The resistors are designed to determine the rate at which the voltage is amplified. The higher the resistance, the greater the amplification.

The Op-Amp's output voltage is represented by the measurement of the light intensity incident on the photodiode. This voltage is read and processed by the microcontroller. Fig. 8 details the Op-Amp schematic.

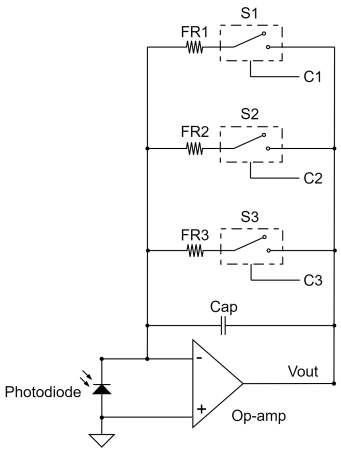

Fig. 8. Schematic of the TIA.

As detailed, the feedback resistors (FR) are important for amplifying the signal through the Op-Amp. It is therefore crucial to design them in such a way as to meet the values that promote this amplification. To design the FRs, a simulation environment was initially developed using Psim software.

During the simulation, the Op-Amp was supplied with a voltage of 5 V. In this way, the Vout voltage can vary from 0 V to 5 V. When saturation occurs in the Op-Amp, the FRs are triggered.

The feedback resistors have an equation that relates the voltage and power variables in dBm. The equation 2 defines this relationship between voltage and power.

$$P_{dbm} = a \cdot \ln(V_{OUT}) + b \tag{2}$$

Where: P_{dBm} is the Power of the optical fiber in dBm; "a" and "b" are constant; "ln" is the natural logarithm; and V_{OUT} is the output voltage of the Op-Amp;

Tab. I shows the voltage and power values for each of the feedback resistors.

TABLE I
VALUES OBTAINED IN THE SIMULATION.

Feedback Resistance (Ω)	Simulated Power (dBm)	Voltage (V)
275 k	-15.6	4.85
	-19	2.22
	-22.4	1.01
	-25.8	0.463
	-29.2	0.212
	-32.6	0.0968
13.8 M	-32.6	4.85
	-36	2.22
	-39.4	1.01
	-42.8	0.463
	-46.2	0.212
	-49.6	0.0968
690 M	-49.6	4.84
	-53	2.21
	-56.4	1.01
	-59.8	0.462
	-63.2	0.211

To obtain the values observed in the Tab. I, the FRs were equated using the trial and error method. Initially, the fiber power was measured by an OPM, and then the Vout of the Op-Amp was checked.

In the first measurement, the resistance was adjusted to obtain a voltage close to 5 V, indicating saturation. Next, by cascading splitters, the optical signal was attenuated until the Op-Amp's output voltage approached 0V. When this occurred, the fiber power was maintained and the resistance was adjusted again until it reached approximately 5 V. This process was repeated, with the signal being attenuated until the Op-Amp's output voltage approached 0 V when it reached 5 V.

With the simulations, it was possible to determine the three FRs (FR1, FR2 and FR3), with the following values: 275 kΩ, 13,8 MΩ and 690 MΩ, respectively.

Each feedback resistor is associated with a voltage and power range. When the output voltage reaches a very low value (around 0,0968 V), there is a switch to a larger feedback resistor. This change leads to an increase in the value of the output voltage.

Curves were adjusted to the experimental data relating power (in dBm) and voltage (in V) using a logarithmic function based on equation 2. The data were collected and

organized into three distinct sets, as presented in Fig. 9, 10 and 11. Each data set corresponds to a specific power range.

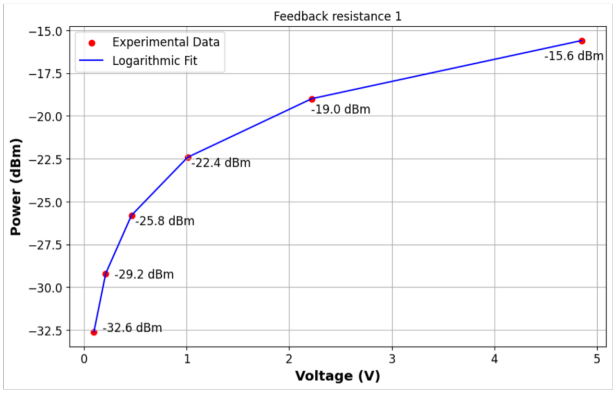

Fig. 9. Feedback resistance 1.

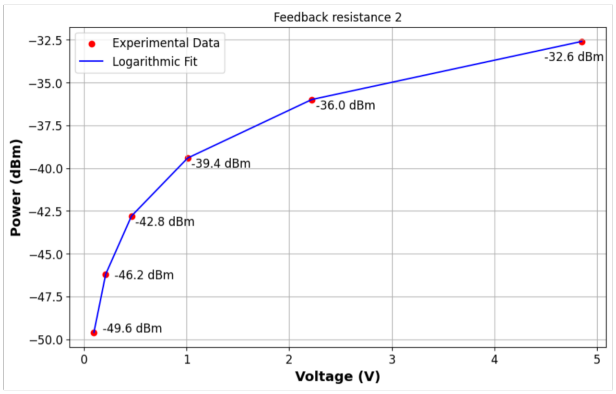

Fig. 10. Feedback resistance 2.

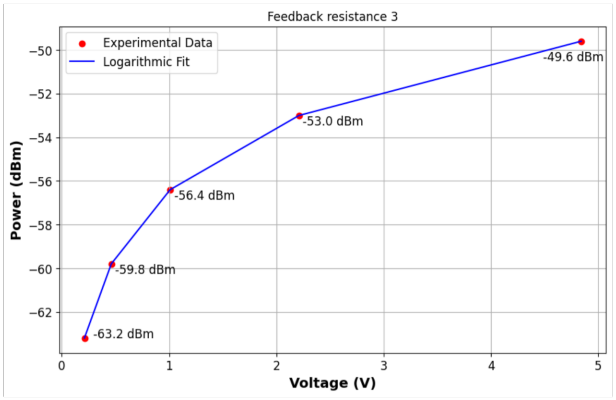

Fig. 11. Feedback resistance 3.

The generated graphs show the fitted curve to the experimental data for each power range. The logarithmic function fitted to each data set effectively models the relationship between power and voltage, highlighting the trend of decreasing voltage as the power becomes more negative.

Tab. II shows the optimized parameters, the standard error and the CRLB of each optimized parameter for the resistance graphs.

TABLE II
GRAPH PARAMETERS FOR EACH RESISTANCE

	Parameter	Resistance 1	Resistance 2	Resistance 3
Optimized parameters	a	4.3436	4.3436	4.3418
	b	-22.4568	-39.4568	-56.4450
Standard error of parameters	a	0.0025	0.0025	0.0009
	b	0.0035	0.0035	0.0010
CRLB	a	0.000006	0.000006	0.000001
	b	0.000012	0.000012	0.000001

The "a" and "b" parameters were optimized during the adjustment for each data set and applied to equation 2 to generate the graphs. Their standard errors were calculated from the covariance matrix. The standard error values indicate the precision of the estimates, while the Cramér-Rao Lower Bound (CRLB) provides theoretical limits for the variance of the estimators. The comparison between the standard errors and the CRLB values suggests that the obtained estimates are efficient since the standard errors are close to the established limits.

C. Microcontroller

The microcontroller is responsible for switching the feedback resistors. The algorithm handles tasks ranging from pin configurations to serial communication settings and initializing the LoRa module, which is used to send data to the gateway.

The flowchart in Fig. 12 details the microcontroller's processing stage in order to control and communicate with the device.

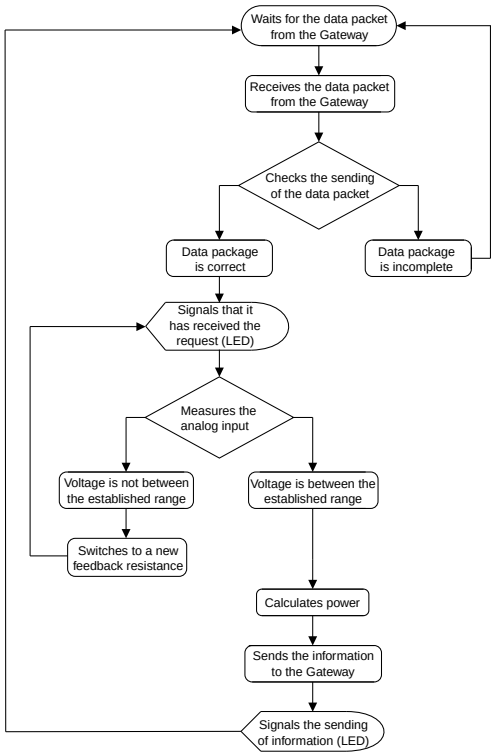

Fig. 12. Flowchart with System Logic.

D. Simulation

The next stage in the system's development was simulation testing, in order to validate the theories discussed. At this

stage, the electrical diagrams were developed using Psim simulation software.

To simulate the photocurrent generated by the photodiode, a current source and the photodiode's electronic schematic with parasitic interference (capacitances and inductances) were used. According to [27], this interference results from factors such as wire connections and conductor structures, which in photodetector systems have an impact on the connection. The Fig. 13 details the circuit.

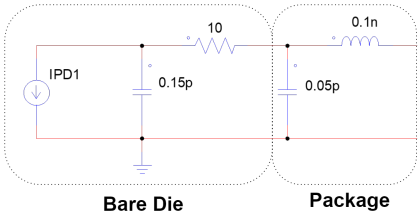

Fig. 13. Simulation squematic.

The values used in the Fig. 13 were taken from [27]. According to [27], the average value of the photogenerated current is found using Equation 3.

$$I_{Pd} = R_{es}.P \tag{3}$$

Where P is defined by:

$$P = 10^{(P_{dBm}-30)/10} \tag{4}$$

Where: I_{Pd} is the photodetector current; R_{es} is the responsivity of the photodetector (A/W); P is the optical power (W); and P_{dBm} is the Power of the optical fiber in dBm.

The op-amp used in the simulation was the MCP601, details of which can be found in [28]. The configuration parameters for the op-amp simulation were as follows: input Resistance of 10^12 Ω; DC Gain A0 of 5.623k; Unity Gain Frequency of 2.8 MHz; Output Resistance of 80 Ω; Maximum Output Current of 30 mA; VCC of 5 V; and VEE of 0 V.

Based on this information, the circuit in Fig. 14 was built. The average photogenerated current was calculated according to Equations 4 and 3, respectively. The responsivity used is approximately 0.64 A/W (data obtained for a wavelength of 1490 nm, from the p-i-n InGaAs photodiode model MTPD1346D-100 [31]), and the optical power (in dBm) responsible for generating the average photogenerated current is based on Fig. 7, considering an attenuation of -21.6 dB.

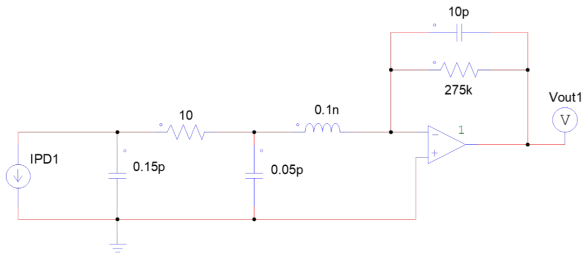

Fig. 14. TIA scheme in Psim.

The output voltage values of the operational amplifier using a feedback resistance of 275 kΩ are shown in the graph in Fig. 15. For V_{out1}, a value of -15,6 dBm was used, for V_{out2} it was -19 dBm and then the signal was gradually attenuated by 3,4 dB, reaching V_{out6} with a power value of -32,6 dBm.

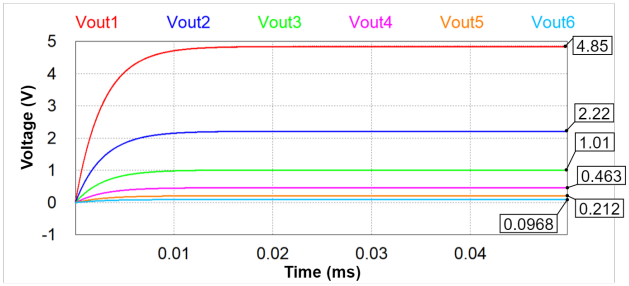

Fig. 15. Voltages obtained with FR of 275kΩ.

After the voltage V_{out6} reaches a low value (in this case 0.0968 V), a new resistor is inserted to adjust the output voltage close to 5 V. The feedback resistors used for the different power values are shown in Tab. III.

TABLE III
SIMULATED VOLTAGE VALUES FROM FEEDBACK RESISTORS.

Feedback resistance (Ω)	Power (dBm)	Power (W)	IPD average (A)	Voltage (V)
275 k	-15.6	27.5423 µ	17.6271 µ	4.85
	-19	12.5893 µ	8.05712 µ	2.22
	-22.4	5.7544 µ	3.68282 µ	1.01
	-25.8	2.63027 µ	1.68337 µ	0.463
	-29.2	1.20226 µ	769.449 n	0.212
	-32.6	549.541 n	351.706 n	0.0968
13,8 M	-32.6	549.541 n	351.706 n	4.85
	-36	251.189 n	160.761 n	2.22
	-39.4	114.815 n	73.4818 n	1.01
	-42.8	52.4807 n	33.5877 n	0.463
	-46.2	23.9883 n	15.3525 n	0.212
	-49.6	10.9648 n	7.01746 n	0.0968
690 M	-49.6	10.9648 n	7.01746 n	4.84
	-53	5.01187 n	3.2076 n	2.21
	-56.4	2.29087 n	1.46616 n	1.01
	-59.8	1.04713 n	670.162 p	0.462
	-63.2	478.63 p	306.323 p	0.211

The simulation showed satisfactory results, allowing the values of the feedback resistors required to take power readings ranging from -15,6 dBm to -63,2 dBm to be determined.

E. Prototype Construction

After defining the components, developing the algorithm and the equation, the process of developing the final prototype began.

The board was developed using KiCAD prototyping software and designed to incorporate the Op-Amp (MCP601), feedback resistors, Arduino Nano (Microcontroller), switching integrated circuit (CD4066B), LoRa module, resistors, capacitors and voltage input sources. Fig.16 details the 3D prototype in KiCAD software.

After developing the circuit for the final prototype using KiCAD prototyping software, the board was made using an LPKF model E33 plotter and its components were soldered in the laboratory. With the physical construction of the prototype, it was possible to carry out tests in the laboratory to validate the circuit. The device board is shown in Fig. 17.

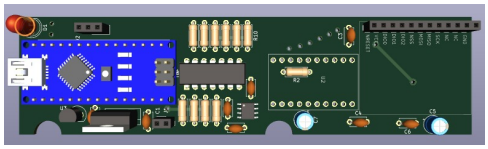

Fig. 16. 3D prototype in KiCAD.

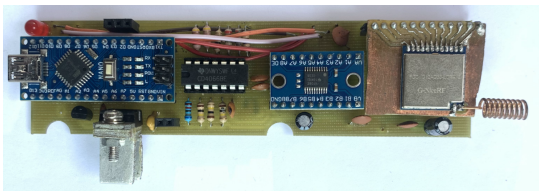

Fig. 17. Final prototype.

F. Gateway

A gateway was developed for communication with a fiber optic central station. Whenever optical power is requested from the prototype, the signal is received, the power is measured, and the measured value is sent to the Gateway.

The gateway system was developed using an Arduino Nano V3, a bidirectional converter, a NiceRF 1276 LoRa module and an ESP WiFi LoRa 32 (V2). Fig. 18 details the Gateway system.

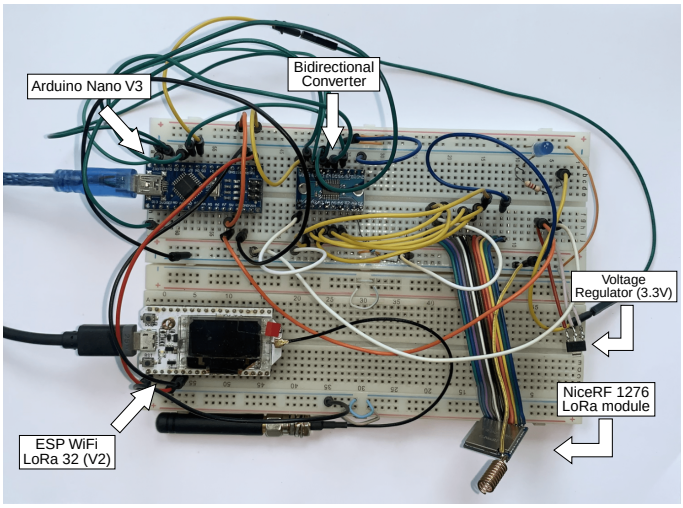

Fig. 18. Gateway hardware.

IV. RESULTS

After the simulation, bench tests, design and assembly of the final prototype, the device was tested in optical networks to validate its functionality. Splitters were combined to obtain a signal range that simulates the scenario in the field, where there are losses such as connection losses, fiber mileage losses and optical splice box losses.

A cascading system of 1/16 and 1/8 splitters was used to simulate the 1% power directed to the measurement device. After this configuration, the power emitted by the OLT was measured, and a value of 5.4 dBm was recorded. The value measured by the OPM, after the splitter cascading system simulating the 1% power, was -18.86 dBm, resulting in a total loss of -24.26 dB. Fig. 19 details the process of cascading the splitters used to attenuate the power of the signal from the OLT. After this process, the -18.86 dBm signal is attenuated (signal attenuation block) and measured by the device.

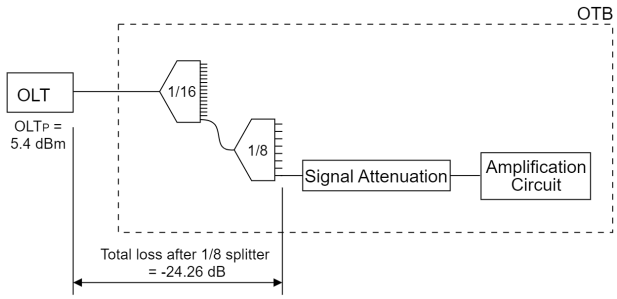

Fig. 19. Signal attenuation with splitters cascading.

Three feedback resistors were defined for the final prototype. The resistors used in the final device differed from those used in the simulation due to three factors: the actual power values emitted by the OLT were different from the simulated values; the simulation used the characteristics of a conventional p-i-n photodiode; and the actual values of parasitic capacitances and inductances differed from those adopted in the simulation. Therefore, the feedback resistors applied to the final prototype have the following values: 368 kΩ, 16.4 MΩ and 500 MΩ, which correspond to FR1, FR2 and FR3, respectively. To obtain these resistance values, commercial resistors connected in series or parallel were applied.

The feedback resistors used were subjected to the same techniques and methods as the resistors used in the simulation. In this case, potentiometers were used to find the feedback resistors by the method of trial and error. The voltage and power values used to generate the logarithmic curve equation are shown in Tab. IV.

TABLE IV
VALUES OBTAINED WITH THE FINAL DEVICE AND OPM

Feedback resistance (Ω)	Voltage (V)	Power measured by the OPM (dBm)
368 k (100k + 100k + 100k + 68k)	4.13	-18.86
	2.32	-21.4
	1.09	-23.8
	0.48	-27.18
	0.24	-30.13
	0.09	-34.02
16.4 M (1M + 2.7M + 2.7M + 10M)	4.32	-34.7
	2.49	-36.9
	1.17	-40.4
	0.63	-43.4
	0.26	-47
	0.12	-49.8
500 M (1 G // 1 G)	3.62	-49.8
	1.93	-52.38
	0.87	-55.98
	0.35	-59.7
	0.13	-63.8

The analysis of the three resistors revealed that the logarithmic adjustment applied to the experimental voltage and power data is effective, as evidenced by the optimized parameters and statistical metrics shown in Tab. V.

TABLE V
GRAPH PARAMETERS FOR EACH DEVICE RESISTANCE

	Parameter	Resistance 1	Resistance 2	Resistance 3
Optimized parameters	a	3.9393	4.2907	4.2217
	b	-24.4388	-41.0344	-55.2468
Standard error of parameters	a	0.0702	0.0968	0.0399
	b	0.0955	0.1219	0.0485
CRLB	a	0.0049	0.0094	0.0016
	b	0.0091	0.0149	0.0024

The values of the optimized parameters show relatively low standard errors, indicating the accuracy of the estimates. In addition, the coefficients of variance of the estimator (CRLB) are equally low, confirming the efficiency of the estimators and the reliability of the adjusted parameters. This combination of low standard errors and low CRLB reinforces the robustness of the adjustments made and ensures the accuracy of the logarithmic model applied to the experimental data.

The final prototype needs to notify the gateway of the power reaching the user. To do this, it is necessary to disregard the 24.26 dB attenuation caused to simulate the 1% power directed to the measurement device.

Thus, by using the three feedback resistors and adding the 24.26 dB to each equation, it is possible to get a power range between -42.86 dBm and 5.41 dBm (see Tab.VI). The feedback resistor equations used in the microcontroller code are:

$$P_{dbm} = (3.9393 \cdot \ln(V_{OUT}) - 24.4388) + 24.26 \quad (5)$$

$$P_{dbm} = (4.2907 \cdot \ln(V_{OUT}) - 41.0344) + 24.26 \quad (6)$$

$$P_{dbm} = (4.2217 \cdot \ln(V_{OUT}) - 55.2468) + 24.26 \quad (7)$$

After all the adjustments made for the final tests, and using equations 5, 6 and 7, it was possible to determine the power of the signal that the OLT is sending to the OTB and splitter where it is installed. This allows us to detect any problems that may be occurring with the client. The values measured by the final prototype after it was requested by the gateway are shown in Tab. VI.

According to [32], the lowest power range that the PON (Rx Sensitivity) port can measure is -32 dBm. Power below this value indicates possible irregularities in the client's optical network. Among the problems are the bad connection between the splitters, curves in the optical fiber above what is allowed or possibly even a break in the fiber.

To check the reliability of the device, a measurement test was made comparing the value measured by the sensor and the value measured by the OPM. The result of this comparison is shown in Tab. VII.

TABLE VII
COMPARING DEVICE AND OPM MEASUREMENTS.

Power measured by the device (dBm)	Power measured by the OPM (dBm)	Relative error percent (%)
-18.85	-18.86	0.04
-21.12	-21.4	1.29
-24.10	-23.8	1.26
-27.33	-27.18	0.55
-30.06	-30.13	0.23
-33.92	-34.02	0.28
-34.76	-34.7	0.16
-37.12	-36.9	0.60
-40.36	-40.4	0.10
-43.02	-43.4	0.88
-46.81	-47	0.40
-50.13	-49.8	0.67
-49.82	-49.8	0.03
-52.47	-52.38	0.17
-55.83	-55.98	0.26
-59.68	-59.7	0.04
-63.86	-63.8	0.09
-67.12	NO READING	-

Tab. VII shows that the relative errors between the measurements made by the device and the OPM are very small. The largest margin of error was just 1.29%. During the measurements, the device was able to capture a power of -67.12 dBm, while the OPM saturated and was unable to take this measurement. These results indicate the effectiveness and reliability of the device, highlighting its ability to provide accurate measurements compared to the OPM. The consistency between the measured values reinforces the validity and usefulness of the device in optical power measurement in fiber optic systems.

V. CONCLUSION

After making the adjustments, it was possible to carry out the tests and see that the system proposed and developed in

TABLE VI
POWER SENT BY FINAL PROTOTYPE TO GATEWAY

Feedback resistance (Ω)	Attenuation before splitter cascading (dB)	Cascading Splitters					Voltage (V)	Power sent to gateway (dBm)
368 k (100k + 100 k+ 100k + 68k)	-24.26	No					4.13	5.41
		1/2					2.32	3.14
		1/4					1.09	0.16
		1/8					0.48	-3.07
		1/16					0.24	-5.80
16.4 M (1M + 2.7M + 2.7M + 10M)		1/16	1/2				0.09	-9.66
		1/16	1/2				4.32	-10.50
		1/16	1/4				2.49	-12.86
		1/16	1/8				1.17	-16.10
		1/16	1/16				0.63	-18.76
		1/16	1/16	1/2			0.26	-22.55
		1/16	1/16	1/4			0.12	-25.87
500 M (1 G // 1 G)		1/16	1/16	1/4			3.62	-25.56
		1/16	1/16	1/8			1.93	-28.21
		1/16	1/16	1/8	1/2		0.87	-31.57
		1/16	1/16	1/8	1/4		0.35	-35.42
		1/16	1/16	1/8	1/8		0.13	-39.60
		1/16	1/16	1/8	1/8	1/2	0.06	-42.86

this research has advantages compared to commercial devices. The main difference lies in the power range achieved by the proposed system, where the device was able to measure a range of -42.86 dBm to 5.41 dBm, showing its efficiency in capturing the possible losses caused in the field.

In addition to this, the system has an interface that allows the user to be informed of the value of the power measured in their fiber optic network whenever necessary. This processing takes place via the gateway. It is worth noting that the system is classified as intelligent, falling into the category of IoT devices.

The device enables remote monitoring during maintenance. It is capable of transmitting power data remotely, which saves time and labor while enabling real-time analysis of the network's status.

This article presents a proposed system that stands out for its innovation and its potential for optimizing optical systems. The results obtained demonstrate the system's effectiveness and applicability, contributing significantly to advances in the field of optical systems.

For future work, the device will be improved to use the ESP LoRa embedded system, making adjustments to the system's power supply to accommodate the embedded system. Changing the microcontroller will reduce costs, since the system will have the microcontroller and LoRa integrated into a single embedded system.

The prototype was developed to be inserted into OSBs, measuring the power of the optical fiber whenever requested or when there is a network failure. In future work, the intention is to create a smaller prototype, capable of being accommodated inside the OSB. We also want to conduct tests to optimize energy savings and make current adjustments based on the temperature sensor's readings.

REFERENCES

[1] Khater, Mostafa M. A. "Multi-vector with nonlocal and non-singular kernel ultrashort optical solitons pulses waves in birefringent fibers". Chaos, Solitons & Fractals, vol. 167, 2023, p. 113098. ScienceDirect, doi: www.doi.org/10.1016/j.chaos.2022.113098.

[2] Kao, K. Charles, and George A. Hockham. "Dielectric-fibre surface waveguides for optical frequencies." Proceedings of the Institution of Electrical Engineers. Vol. 113. No. 7. IET Digital Library, 1966. doi: www.doi.org/10.1049/piee.1966.0189.

[3] Al-Tarawneh, Luae, et al. "Evolution of Optical Networks: From Legacy Networks to next-Generation Networks". Journal of Optical Communications, vol. 44, nº s1, 2024, p. s955–70. doi: www.doi.org/10.1515/joc-2020-0108.

[4] Oughton, Edward J., et al. "Policy choices can help keep 4G and 5G universal broadband affordable". Technological Forecasting and Social Change, vol. 176, 2022, p. 121409. ScienceDirect, doi: www.doi.org/10.1016/j.techfore.2021.121409.

[5] Gu, Rentao, et al. "Machine learning for intelligent optical networks: A comprehensive survey". Journal of Network and Computer Applications, vol. 157, 2020, p. 102576. ScienceDirect, doi: www.doi.org/10.1016/j.jnca.2020.102576.

[6] Shao, Chen, et al. "Machine Learning in Short-Reach Optical Systems: A Comprehensive Survey." 2024. doi: www.doi.org/10.48550/arXiv.2405.09557.

[7] Nyarko-Boateng, Owusu, et al. "Fiber Optic Deployment Challenges and Their Management in a Developing Country: A Tutorial and Case Study in Ghana". Engineering Reports, vol. 2, no 2, 2020, p. e12121. doi: www.doi.org/10.1002/eng2.12121.

[8] Karar, Abdullah S., et al. "Recent Advances in Coherent Optical Communications for Short-Reach: Phase Retrieval Methods". Photonics, vol. 10, no 3, 2023, p. 308. MDPI, doi: www.doi.org/10.3390/photonics10030308.

[9] Zhang, Junwen, e Zhensheng Jia. "Coherent Passive Optical Networks for 100G/γ-and-Beyond Fiber Access: Recent Progress and Outlook". IEEE Network, vol. 36, no 2, 2022, p. 116–23. IEEE Xplore, doi: www.doi.org/10.1109/MNET.005.2100604.

[10] Velychko, Oleh, et al. "Features of the Calibration of Optical Power Meters". 2022 XXXII International Scientific Symposium Metrology and Metrology Assurance (MMA), 2022, p. 1–4. IEEE Xplore, doi: www.doi.org/10.1109/MMA55579.2022.9992606.

[11] Sun, Jian. "Design and research of wireless optical power meter based on IoT big data and physical quantity". Results in Physics, vol. 54, 2023, p. 107045. ScienceDirect, doi: www.doi.org/10.1016/j.rinp.2023.107045.

[12] Mekki, Kais, et al. "A comparative study of LPWAN technologies for large-scale IoT deployment." ICT express 5.1 (2019): 1-7. ScienceDirect, doi: www.doi.org/10.1016/j.icte.2017.12.005.

[13] Gu, Fei, et al. "Survey of the low power wide area network technologies." Journal of Network and Computer Applications 149 (2020): 102459. ScienceDirect, doi: www.doi.org/10.1016/j.jnca.2019.102459.

[14] Zanaj, Eljona, et al. "Energy efficiency in short and wide-area IoT technologies—A survey." Technologies 9.1 (2021): 22. MDPI, doi: www.doi.org/10.3390/technologies9010022.

[15] Singh, Ritesh Kumar, et al. "Energy consumption analysis of LPWAN technologies and lifetime estimation for IoT application." Sensors 20.17 (2020): 4794. MDPI, doi: www.doi.org/10.3390/s20174794.

[16] Ertürk, Mehmet Ali, et al. "A survey on LoRaWAN architecture, protocol and technologies." Future internet 11.10 (2019): 216. MDPI, doi: www.doi.org/10.3390/fi11100216.

[17] Abdellaoui, Zouhaira, et al. "Design, implementation and evaluation of a Fiber To The Home (FTTH) access network based on a Giga Passive Optical Network GPON". Array, vol. 10, 2021, p. 100058. ScienceDirect, doi: www.doi.org/10.1016/j.array.2021.100058.

[18] Nesset, Derek. "Next Generation PON Technologies: 50G PON and Beyond (Invited)". 2023 International Conference on Optical Network Design and Modeling (ONDM), 2023, p. 1–6. IEEE Xplore, Available: www.ieeexplore.ieee.org/abstract/document/10144842.

[19] Dias, Leonardo Pereira, et al. "Evolutionary Strategy for Practical Design of Passive Optical Networks". Photonics, vol. 9, nº 5, 2022, p. 278. doi: www.doi.org/10.3390/photonics9050278.

[20] Cheng, Lin, et al. "A U-shaped-wound fiber macro-bending loss crack sensor improved by an optical splitter". Optical Fiber Technology, vol. 58, 2020, p. 102259. ScienceDirect, doi: www.doi.org/10.1016/j.yofte.2020.102259.

[21] Pereira, Francisco Carlos De Lima, e Edgard Jamhour. "Proposal for an Algorithm for Positioning of Splitter Optical Power to Networks GPON". Brazilian Journal of Development, vol. 7, nº 4, 2021, p. 43454–64. doi: www.doi.org/10.34117/bjdv7n4-687.

[22] Bazakutsa, Pavel V., et al. "Fused optical couplers: power transfer between optical fibers". 2022 4th International Youth Conference on Radio Electronics, Electrical and Power Engineering (REEPE), 2022, p. 1–5. IEEE Xplore, doi: www.doi.org/10.1109/REEPE53907.2022.9731448.

[23] Zeng, Tao, et al. "China Telecom's Research and Applications of Business-Enterprise Full-Optical Networking". IEEE Access, vol. 11, 2023, p. 55824–33. IEEE Xplore, doi: www.doi.org/10.1109/ACCESS.2023.3239882.

[24] Serečunová, Stanislava, et al. "Design and Optimization of 1 × 2 Y-Branch Optical Splitters for Telecommunication Applications". Journal of Electrical Engineering, vol. 71, nº 5, 2020, p. 353–58. sciendo.com, doi: www.doi.org/10.2478/jee-2020-0048.

[25] Kacus, Hatice, et al. "Phenol red based hybrid photodiode for optical detector applications". Solid-State Electronics, vol. 171, 2020, p. 107864. ScienceDirect, doi: www.doi.org/10.1016/j.sse.2020.107864.

[26] Olantera, Lauri, et al. "Radiation Effects on High-Speed InGaAs Photodiodes". IEEE Transactions on Nuclear Science, vol. 66, nº 7, 2019, p. 1663–70. IEEE Xplore, doi: www.doi.org/10.1109/TNS.2019.2902624.

[27] Säckinger, Eduard. *Analysis and design of transimpedance amplifiers for optical receivers*. John Wiley & Sons, 2017. ISSN: 978-1119263753.

[28] Microchip Technology. "MCP601/1R/2/3/4." [Online]. Available: ww1.microchip.com/downloads/en/DeviceDoc/21314g.pdf.

[29] Liya, M. L., e M. Aswathy. "LoRa technology for Internet of Things (IoT): A brief Survey". 2020 Fourth International Conference on I-SMAC (IoT in Social, Mobile, Analytics and Cloud) (I-SMAC), 2020, p. 8–13. IEEE Xplore, doi: www.doi.org/10.1109/I-SMAC49090.2020.9243449.

[30] Furukawa Electric LatAm. "1XN TAPERED OPTICAL SPLITTER." 2021, [Online]. Available: www.furukawalatam.com/en_US/versao-et-pdf/1xn-tapered-optical-splitter.

[31] OPTOELECTRONICS. "InGaAs PIN Photodiode Datasheet." 2021. Available: www.mouser.in/datasheet/2/1094/MTPD1346D_100-1900758.pdf.

[32] VSOL. "16 Port EPON OLT." 2023. [Online]. Available: flytec.com.py/download/files/VSOL%20EPON%20L3%20OLT%20DataSheet%20V1_4.pdf.

VI. Biography Section

Danillo Fernandes do Nascimento was born in Cariré, Ceará, Brazil, on December 3, 1995. He received his Bachelor's degree in Electrical Engineering from the Federal University of Ceará, Brazil, in 2020. He is currently a master's student in the Graduate Program in Electrical and Computer Engineering (PPGEEC) at the Federal University of Ceará. His research interests include analog electronics, power electronics, green hydrogen, optical system and embedded systems.

Italo Rossi Araújo Costa was born on August 3, 1990, in Itapipoca, Ceará, Brazil. He earned a Bachelor's degree in Computer Science from the State University of Vale do Acaraú in Sobral, Ceará, Brazil, in 2013. He holds a specialization in Networks and Systems Security from the Inta University Center (UNINTA) in Sobral, Ceará, since 2016, and also a specialization in Computer Forensics and Digital Forensics from the Institute of Postgraduate and Graduate Studies in Fortaleza, Ceará, since 2020. Between 2018 and 2023, he achieved various Furukawa certifications focused on Fiber Optic Networks and PON Network Projects. Italo has been working in the Fiber Optic Networks field since 2013 and currently serves as the Coordinator of Network Infrastructure at an ISP in Sobral, Ceará. He is currently a master's student in the Graduate Program in Electrical and Computer Engineering (PPGEEC) at the Federal University of Ceará. His research interests include Artificial Intelligence applied to the Financial Market, Optical Fibers, and PON Networks.

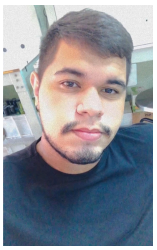

Rhuan da Silva Nunes was born in Sobral, Ceará, Brazil, on October 21, 1997. He received his Technologist degree in Industrial Mechatronics from the Federal Institute of Ceará, Brazil, in 2023. Also in 2023, he completed a Specialization in Technologies for Professional and Technological Education at the Federal Institute of Santa Catarina, Brazil. He is currently a master's student in the Graduate Program in Electrical and Computer Engineering (PPGEEC) at the Federal University of Ceará. His research interests include analog electronics, embedded systems, optical systems, educational technologies and active methodologies.

José Cláudio do Nascimento was born in Fortaleza, Brazil, in 1980. He received the B.Sc. degree in electrical engineering, the M.Sc. degree in teleinformatic engineering, and the Ph.D. degree in teleinformatic engineering from the Universidade Federal do Ceará–UFC, Brazil, in 2005, 2006, and 2009, respectively. He is currently a Professor of quantum information and optics communications with the Electric Engineering Department, Universidade Federal do Ceará–UFC–Campus Mucambinho, Sobral, Brazil.